Processing of Hierarchical Structures on Stainless Steel by Direct Laser Interference Patterning

Hidenori Shimada, Kyohei Watanabe, and Masaki Yamaguchi*

Graduate School of Medicine, Science & Technology, Shinshu University, 3-15-1, Tokida, Ueda 386-8567, Japan
**Corresponding author's e-mail: masakiy@shinshu-u.ac.jp*

The purpose of this study was to establish a method for fabricating both nano- and microscale texturing that allows for any pitch and depth with direct laser interference patterning using a liquid crystal on silicon-spatial light modulator (LCOS-SLM). Three types of periodic structures, 780 nm of nanoscale, microscale (10 – 30 μm), and hierarchical, were fabricated on stainless steel using a femtosecond-pulsed laser by adjusting the number of repetition shots and their pitch. The measured pitches of the two-beam laser interference agreed well with the calculated values. The experimental data demonstrated that it was possible to process hierarchical structures by an optical unit for interference patterning that could produce patterns with any pitch and depth. The pitch of the periodic structures was controlled by the diffraction angle, and their depth was controlled by the number of repetition shots. In the proposed optical unit, a mask containing multiple holes was an essential component for the LCOS-SLM to block the harmonic waves in the subsequent laser interference. The coefficient of variation of the apparent contact angle was smaller for the hierarchical structures than for the microscale periodic structures. The hierarchical structures on stainless steel had a hydrophobicity of over 136° with good stability.

DOI: 10.2961/jlmn.2021.02.2004
Keywords: laser interference, femtosecond-pulsed laser, nano/microscale surface topography, direct laser interface patterning, liquid crystal on silicon-spatial light modulator, hierarchical structure, hydrophobicity

1. Introduction

Nature-inspired biomimetic surfaces have been developed with improved physical properties for applications such as liquid repellency, low adhesion, self-cleaning, and drag reduction. Such surfaces are described as having functional textures [1,2]. In particular, hydrophobic surfaces, whose apparent contact angle with water is 120°, such as perfluorinated materials, can be produced by mimicking lotus leaves, which possess hierarchical structures with both micro- and nanoscale features [3].

Several fabrication methods have been proposed for producing hierarchical structures, in particular spin coating [4], dispersing of nano-sized beads [5], and lithographic techniques [6-7]. However, a rapid processing method for hierarchical structures with both nano- and microscale features that is applicable for general industrial materials such as steels is yet to be established.

Pulsed laser sources, such as femtosecond-pulsed lasers, have been applied for three-dimensional processing with nano/microscale surface topography in an open environment and in an acceptable time [8-9]. Interference patterning has been proposed for fabricating periodic structures on industrial materials such as metals and resins [10]. Among these techniques, laser induced periodic surface structuring (LIPSS) and direct laser interference patterning (DLIP) are attractive industrial methods for engraving thousands of grooves with widths from a few tens of nanometers up to several tens of micrometers [11]. LIPSS is a self organizing process based on interference between the laser irradiation and surface plasmon polaritons [12]. In contrast, DLIP structures are generated using a special interferometer-based optical setup [13-15]. LIPSS and DLIP differ in their groove periodicity and modulation depth. The modulation depth of DLIP structures is controlled by the number of repetition shots and is several times larger than that of LIPSS [16].

Some researchers have reported the fabrication of hierarchical structures with pulsed lasers [17,18]. However, these methods produce random nanoscale structures rather than periodic structures. Additionally, the pitch and depth of each two-scale periodic structure cannot be changed arbitrarily. Since the conception of the Mach-Zehnder interferometer, many kinds of beam correlators such as the Lloyd's mirror and the transmission beam splitter with Schwarzschild optics have been used for laser interference patterning [19]. In particular, the spatial light modulator may be useful as a beam correlator because of the ease with which it can generate multiple laser interference. However, only a few reports have discussed the application for femtosecond laser processing [20,21].

The purpose of this study was to establish a novel method for processing hierarchical structures with DLIP that allows for any pitch or depth. Firstly, periodic structures of the order of a few hundreds of nanometers or a few tens of micrometers were fabricated by DLIP using a special interferometer-based optical unit with an LCOS-SLM and a mask as the diffractive optical element. Then, hierarchical structures were fabricated by combining these two-scale periodic structures. Their surface geometries and the wetting

behaviors, such as their apparent contact angles, were compared. Finally, we demonstrated the hydrophobicity of hierarchical structures made from stainless steel.

2. Materials and Methods

2.1 Laser processing

A commercial femtosecond-pulsed laser (Pharos-6W, Light Conversion UAB, Vilnius, Republic of Lithuania) provided pulses at an oscillatory wavelength of 515 nm, a pulse width of 277 fs, and a repetition rate of 10 kHz was used for this experiment. An optical unit for DLIP (Fig. 1) comprised (i) an LCOS-SLM (Hamamatsu Photonics K.K., Hamamatsu, Japan), (ii) a collimated lens (f_1 = 201), (iii) a mask with two holes (200 μm in hole diameter), (iv) a beam expander (f_2 = 60.9 and f_3 = 300.0), and (v) an aspheric condensing lens (f_4= 19.6). The incident angle, θ, to the workpiece can be calculated from the diffraction angle, ψ, for the LCOS-SLM as follows:

$$\theta = \tan^{-1}(F \times \tan\psi) \quad (1)$$

where, $F = (f_1 \times f_3)/(f_2 \times f_4) = 50.5$.

The pitch, τ, of the diffraction grating for both nano-and microscale periodic structures is expressed via the wavelength, λ, as follows:

$$\tau = \frac{\lambda}{2\sin\theta} \quad (2)$$

The nano- and microscale periodic structures were produced by two-beam laser interference. The full width at half maximum (FWHM) of the spot diameter at the focal point on the sample surface was calculated as 218 μm for a laser beam quality factor M^2 = 1.1 and an expanded laser beam diameter of 11 mm. A pitch of 780 nm was used for the smaller periodic structure (hereafter referred to as the nanoscale periodic structure) by setting ψ to 0.397° (θ = 19.3° and l = 6.86 mm). Also, pitches of 10, 20, and 30 μm were used for the microscale periodic structures by setting ψ to 0.029° (θ = 1.47°), 0.015° (θ = 0.74°), and 0.010° (θ = 0.50°).

Stainless steel (SUS430, 1 mm of thickness, Ra = 0.03 μm of surface roughness) was used as the material for fabricating test-pieces with periodic structures (3 mm × 3 mm of processing area). Three types of periodic structures, nanoscale, microscale, and hierarchical, were compared by using test-pieces with different numbers of repetition shots, s, and different pitches, τ (Table 1, where the subscripts "n" and "m" indicate the nano- and microscale periodic structures, respectively). The hierarchical structures were fabricated by superimposing a nanoscale periodic structure onto a microscale periodic structure. Figure 2 shows computer generated holograms (CGH) [22] of the phase grating pattern on the LCOS-SLM used for the fabrication of the test-pieces. The CGHs were calculated by an iterative Fourier transform algorithm [23] using the dedicated software for the LCOS-SLM.

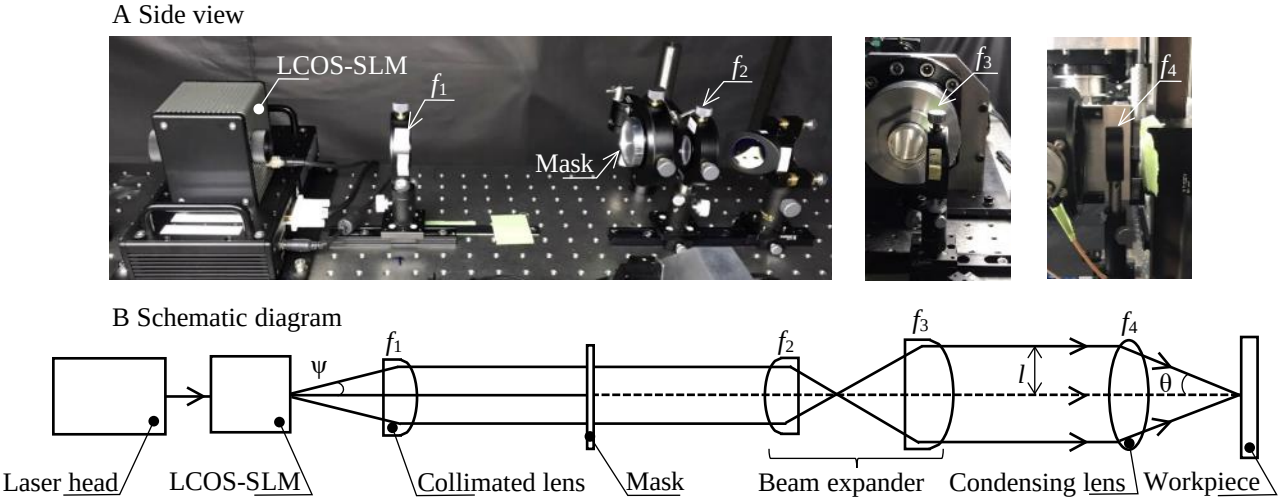

Fig. 1 Configuration of optical unit for interference patterning of DLIP.

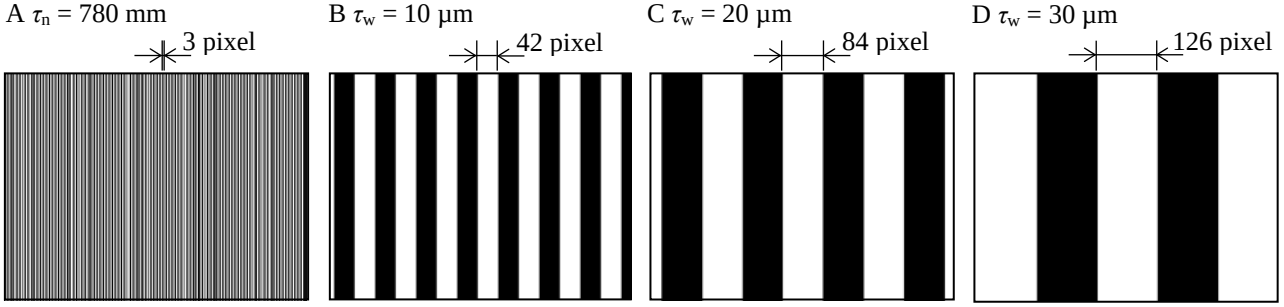

Fig.2 Computer generated hologram of the phase grating pattern used for the fabrication of the test-pieces (pixel: resolution of a liquid crystal used for the LCOS-SLM, □: 2π rad, ■: 0 rad).

The surface geometries of the test-pieces were observed using a non-contact laser confocal microscope (10 nm resolution for depth, OLS4100, Olympus Co., Tokyo, Japan) and a scanning electron microscope (SEM; JEM-6010LA, JEOL Ltd., Tokyo, Japan). Firstly, an average ridgeline was drawn on the plane and side surfaces of the bumps and dents using the dedicated software for the non-contact laser confocal microscope, and the intersection points were obtained. The pitch and depth, *d*, of the periodic structures were then identified from the distances between the intersections points.

The measurements were repeated for 5 times at each point (n = 5). Unless otherwise stated, continuous data are summarized as mean ± standard deviation (SD).

2.2 Simulation of interference patterns

The interference patterns are a function of the number of beams, their phase shift, and their amplitude [24-26]. Interference patterns were simulated numerically as scalar quantities in polar coordinates using the amplitude of each beam, E, the wavenumber, k, the polar angle, θ (= incident angle), the azimuthal angle, ϕ, and the phase shift of the beams, α, as follows:

$$E_n\,(E_{n0}, x, y, z, k_n, \theta_n, \phi_n, \alpha_n, \omega_n, t) = E_{n0}\,\cos\{k_n(-x\sin\theta_n\cos\phi_n - y\sin\theta_n\sin\phi_n + z\cos\theta_n) - \omega_n t + \alpha_n\} \quad (3)$$

where, $\omega = 2\pi c/\lambda$ is the angular velocity and c is the speed of light. The intensity distribution, I, of multiple correlated beams can be expressed as follows:

$$I\,(E_{n0}, x, y, z, k_n, \theta_n, \phi_n, \alpha_n, \omega_n) \propto \int|\sum E(E_{n0}, x, y, z, k_n, \theta_n, \phi_n, \alpha_n, \omega_n, t)|^2\,dt \quad (4)$$

An interference pattern can be simulated by integrating the intensity distribution over a cycle, $\Delta t = \lambda/c$.

2.3 Measurement of wetting behaviors

To evaluate the wettability, the equilibrium contact angle, θ_{cta}, and apparent contact angle, θ'_{cta}, of the test-pieces were measured using a commercial contact angle analyzer (DM-701, Kyowa Interface Science Co. Ltd., Niiza, Japan). A microsyringe was used to place a droplet of distilled water of volume 2 μL onto each test-piece. The measurements of θ_{cta} and θ'_{cta} were repeated five times (n = 5), and the mean values were used.

3. Results and Discussion

3.1 Comparison between calculated and measured patterns

Figure 3 shows a comparison between the calculated and measured two-dimensional top views of the three types of periodic structure. The color bar shows the normalized intensity distribution (in arbitrary units; a.u.) for the calculated values. Periodic structures that can act as a linear diffraction grating were observed for all of the fabricating conditions. The calculated two-dimensional top views of the hierarchical structure are the same as those of the nanoscale periodic structure (A) and the microscale periodic structure (B). Table 2 shows the measured results of the surface geometries, where τ is the pitch of the periodic structure and d is the depth of the periodic surface structure (again, the subscripts

Table1 Conditions of test-pieces with nano- and microscale periodic structures fabricated by two-beam laser interference for wettability evaluation

Sample no.	Pitch τ_n (nm)	Shots s_n	Pitch τ_w (μm)	Shots s_w	Fluence F (mJ/cm^2)
1	780	30	—	—	43
2		50			
3		100			
4	—	—	10	100	35
5				900	
6	—	—	20	100	
7				900	
8	—	—	30	100	
9				900	
10	780	50	10	100	43 (nano-scale)
11		100		100	
12		50		900	
13		100		900	
14	780	50	20	100	
15		100		100	
16		50		900	
17		100		900	
18	780	50	30	100	35 (micro-scale)
19		100		100	
20		50		900	
21		100		900	

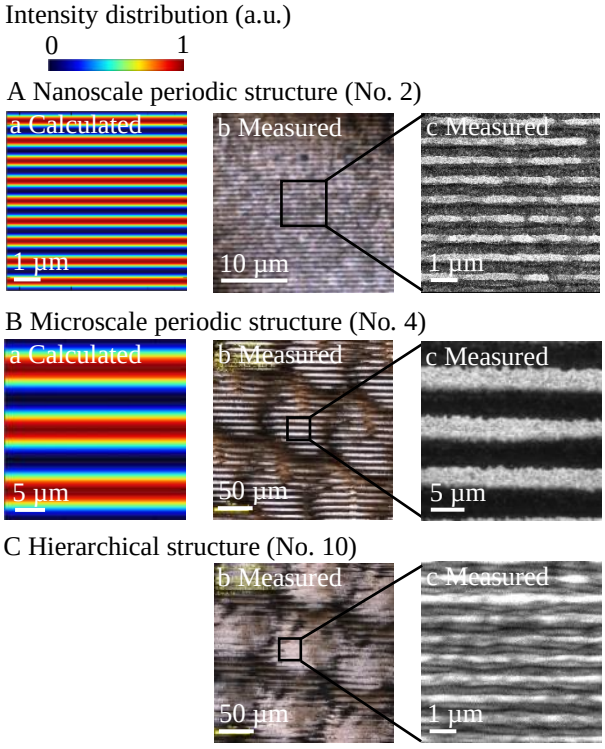

Fig. 3 Comparison between fabricated and calculated two-dimensional top views of three types of periodic structures for two-beam laser interference: (b) measured using a non-contact laser confocal microscope, (c) SEM images.

Table 2 Measured results of the surface geometries for the three types of periodic structures fabricated by two-beam laser interference

$n = 5$

Sample no.	τ_n (nm)	d_n (μm)	τ_m (μm)	d_m (μm)	θ'_{cta}* (°)
1	728	0.154	—	—	103.7
2	728	0.199	—	—	112.7
3	733	0.199	—	—	113.7
4	—	—	9.6	1.38	129.8
5			9.6	7.93	137.3
6	—	—	19.4	1.99	127.7
7			19.3	11.51	136.6
8	—	—	24.1	1.79	131.0
9			24.3	11.93	136.8
10	723	0.311	9.6	1.26	123.4
11	729	0.321	9.5	1.70	133.4
12	723	0.196	9.7	7.51	134.2
13	727	0.274	9.7	7.19	136.1
14	715	0.307	19.2	1.74	129.7
15	716	0.261	19.1	1.74	136.0
16	714	0.188	19.2	10.57	133.7
17	719	0.238	19.1	11.19	135.4
18	712	0.269	24.4	1.59	130.2
19	716	0.327	24.3	1.66	130.8
20	712	0.219	24.4	11.39	133.2
21	718	0.294	24.3	11.52	135.1

* The mean value of equilibrium contact angle of unprocessed surface was 89.6° (n = 21), and the apparent contact angle were measured two weeks after processing.

"n" and "m" indicate the nanoscale and microscale periodic structures, respectively). It was difficult to distinguish between the width of the solid-liquid interface (tooth width) and the width of the liquid-air interface (groove width) because the cross-sectional view had a sinusoidal shape (nanoscale periodic structures) or an acute triangular shape (10 μm of microscale periodic structures).

In the proposed optical unit, the mask with multiple holes was effective in blocking harmonic waves for the subsequent laser interference. The cause of the harmonic waves was considered to be the nonlinearity of the liquid crystal-control voltage characteristics of the LCOS-SLM. Therefore, this could be decreased by using a diffraction grating with grooves with a sine wave-shaped cross section. However, this would make it impossible to generate an arbitrary pitch.

For the nanoscale periodic structures, the measured values of τ_n were in the range of 712 – 733 nm whereas the calculated value was 780 nm (Table 2). The variations of the measured values of τ_n were not so large when compared under the same pitch conditions as those of the microscale periodic structures. For the microscale periodic structures, the measured values of τ_m were in the ranges of 9.5 – 9.7, 19.1 – 19.4 μm, and 24.1 – 24.4 μm, while the calculated values were 10, 20, and 30 μm, respectively. Therefore, the measured pitches produced by the two-beam laser interference agreed well with the calculated values.

The depth of the microscale periodic structures, d_m, increased in proportion to the number of repetition shots. This is a point of strength for DLIP when compared to LIPSS. However, in the nanoscale periodic structure, there was a condition that the depth, d_n, did not increase in proportion to the number of repetition shots. It was considered that the entire laser spot had been processed when the number of shots was comparatively large.

Figure 4 shows the measured results for the surface geometries of the three types of periodic structures formed by two-beam laser interference. Unexpectedly, random nanoscale structures were observed on a part of the tops of the convex parts of the microscale periodic structures. However, nanoscale periodic structures were also observed on top of each convex part of the hierarchical structures. Furthermore, nanoscale periodic structures were observed on the bottoms of the grooves when the microscale periodic structures were comparatively shallow.

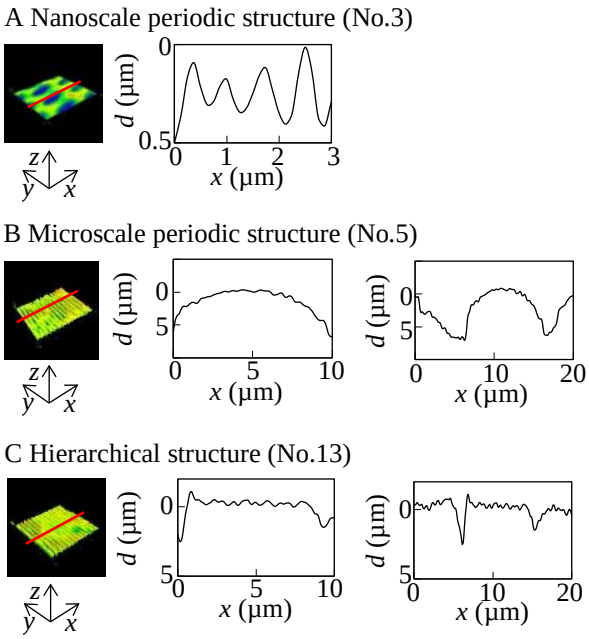

Fig. 4 Measured results for surface geometries of periodic structures fabricated by two-beam laser interference (— : observed sections of surface geometry).

Figure 5 shows the measured results for the diameter of the processing spot for each shot. The maximum diameter in the direction orthogonal to the nanoscale periodic structures was measured. The number of grooves was estimated for the fabricated test-pieces. After 30 shots, the diameter of the processing spot was 56.9 μm, meaning that 78 grooves had been created simultaneously. After 100 shots, the diameter of the processing spot was 64.6 μm, meaning that 88 grooves had been created. Thus, it was shown that around 80 grooves were formed on each spot.

3.2 Wetting behaviors

The mean value of the equilibrium contact angle of the unprocessed surface was 89.6° (n = 21). The apparent contact angles were measured two weeks after processing because it has been reported that the laser processing of metal surfaces creates preferential sites for the adsorption of organic compounds from the air and that the wetting behavior

changes with the amount of carbon on the structured surface [27,28].

The adhesion of distilled water on the fabricated test-pieces was evaluated. Figure 6 shows the measured results from the goniometer images for sample nos. 3, 5, and 13.

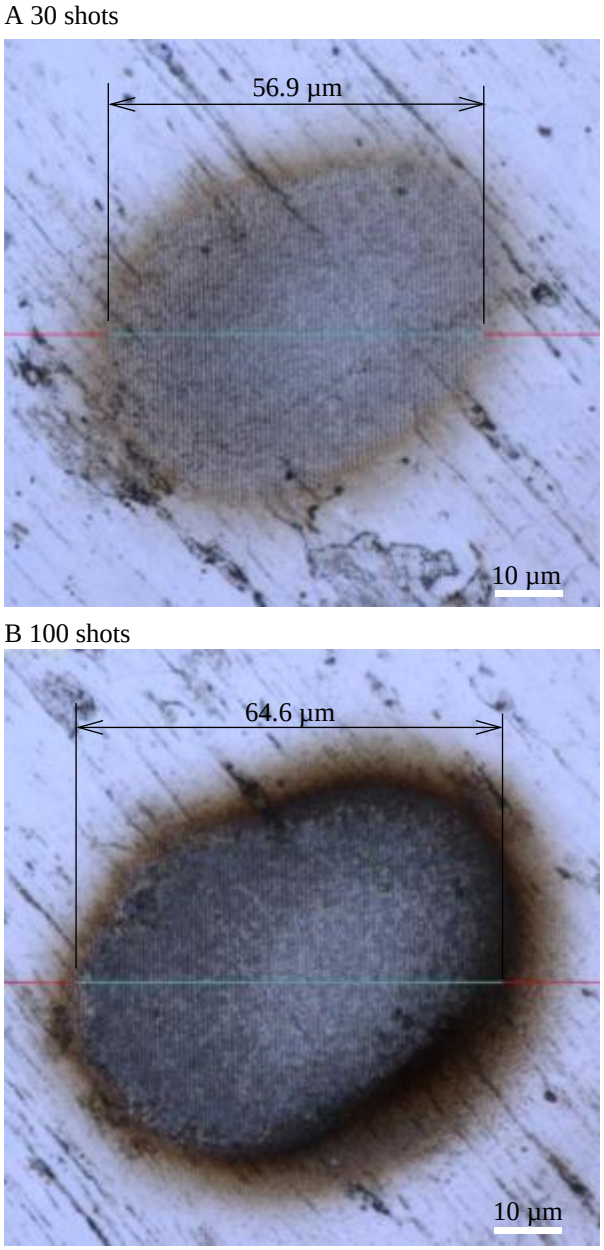

Fig. 5 Measured results for the diameter of processing spot for each shot.

The maximum apparent contact angles were found for each sample, with the largest value of *d*, such as no. 3 for the nanoscale periodic structures, nos. 5, 7, and 9 for the microscale periodic structures, and no.13 for the hierarchical structures (Table 2). These results showed that the water droplet did not reach the bottom of the texture as it was suspended sufficiently to exceed the depth of the DLIP. It has also been reported that periodic structures applied in a uniaxial direction influence the apparent contact angles by less than 2% [29].

Figure 7 shows the apparent contact angles and their coefficients of variation (CVs). Both the microscale and hierarchical structures exhibited an increase in the apparent angles from 89.6° to over 136°, and no significant difference was observed between them. This is because random nanostructures were formed on top of the convex parts of the micro-periodic structures. However, it was considered that the hierarchical structures had smaller CVs and were superior in stability and/or reproducibility. The apparent contact angles of the microscale periodic structures seem to show coincidentally large values. Thus, the hierarchical structures were hydrophobic with good stability.

It was observed in the hierarchical structures that the apparent contact angle tended to decrease slightly with increasing pitch. This phenomenon might be the result of the Cassie-Baxter equation [30,31].

4. Conclusion

The experimental data demonstrated the possibility of processing hierarchical structures by using a femtosecond-pulsed laser with LCOS-SLM for interference patterning of DLIP, which allows for any pitch and depth. The pitch of the periodic structures was controlled by the diffraction angle.

The depth was controlled by the number of repetition shots. A mask with holes was an essential component for the LCOS-SLM to block the harmonic waves in the subsequent laser interference. Hierarchical structures on stainless steel achieved a hydrophobicity of over 136° with good stability. In future work, we would like to examine the upper limit of the number of shots and the linearity with respect to the depth.

Acknowledgments

This work was supported in part by grant no. 20H04514 from the Japan Society for the Promotion of Science, and was based on the ultra-sensitive and rapid cancer testing technique based on fiber-type amplification (Principal Investigator: M. Yamaguchi).

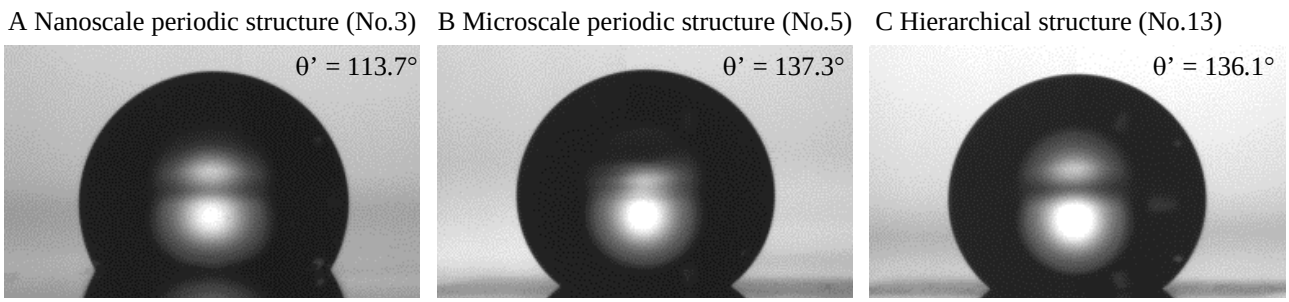

Fig. 6 Measured results of goniometer images for sample nos. 3, 5, and 13.

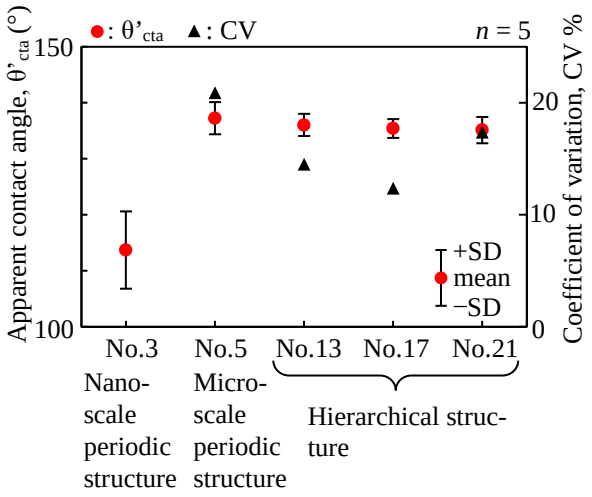

Fig. 7 Comparison of apparent contact angles and their statistical variations.

References

[1] B. Bhushan: Philos. Trans. A Math. Phys. Eng. Sci., 377, (2019) 20180274.

[2] W. Barthlott, M. Mail, B. Bhushan, and K. Koch: Nanomicro Lett., 9, (2017) 23.

[3] B. Bhushan and Y.C. Jung: Prog. Materi. Sci., 56 (2011) 1.

[4] W. Ming, D. Wu, R. van Benthem, and G. de With: Nano Lett., 5, (2005) 2298.

[5] D. Ebert and B. Bhushan: J. Colloid. Interface Sci., 368, (2012) 584.

[6] H. Lee and B. Bhushan: J. Colloid. Interface Sci., 372, (2012) 231.

[7] E. Bittoun and A. Marmur: Langmuir., 28, (2012) 13933.

[8] S. Torres-Peiró, J. González-Ausejo, O. Mendoza-Yero, G. Mínguez-Vega, and J. Lan-cis: Appl. Surf. Sci., 303, (2014) 393.

[9] M-T. Li, M. Liu, and H-B. Sun: Phys. Chem. Chem. Phys., 21, (2019) 24262.

[10] J. Heitz, B. Reisingera, M. Fahrner, C. Romanin, J. Siegel, and V. Svorcik: ICTON 2012, (2012) Tu.B5.2.

[11] J. Bonse: Nanomaterials (Basel), 10, (2020) 1950.

[12] A.K. Jain, V.N. Kulkarni, D.K. Sood, and J.S. Uppal: J. Appl. Phys., 52, (1981) 4882.

[13] A.A. Maznev, T.F. Crimmins, and K.A. Nelson: Opt. Lett., 23, (1998) 1378.

[14] J. Bekesi, J. Meinertz, J. Ihlemann, and P. Simon: Appl. Phys., A. 93, (2008) 27.

[15] P. Graus, T.B. Möller, P. Leiderer, J. Boneberg, and N.I. Polushkin: OE Adv., 3, (2020) 190027.

[16] S. Rung, K. Bokan, F. Kleinwort, S. Schwarz, P. Simon, J-H. Klein-Wiele, C. Esen, and R. Hellmann: Lubricants., 7, (2019) 7050043.

[17] M. Ehrhardt, S. Lai, P. Lorenz, and K. Zimmer: Appl. Surf. Sci., 506, (2020) 144785.

[18] M. Mezera, S. Alamri, W.A.P.M. Hendriks, A. Hertwig, A.M. Elert, J. Bonse, T. Kunze, A.F. Lasagni, and G.R.B.E. Römer: Nanomaterials (Basel)., 10, (2020) nano10061184.

[19] Y. Nakata: Adv. Opt. Techn., 5, (2016) 29.

[20] K. Lou, S.X. Qian, Z.C. Ren, C. Tu, Y. Li, and H.T. Wang: Sci Rep., 3, (2013) 2281.

[21] H. Cheng, P. Li, S. Liu, H. Lu, L. Han, and J. Zhao: Appl. Opt., 59, (2020) 7211.

[22] N. Matsumoto, T. Ando, T. Inoue, Y. Ohtake, N. Fukuchi, and T. Hara: J. Opt. Soc. Am. A., 25, (2008) 1642.

[23] F. Wyrowski and O. Bryngdahl: J. Opt. Soc. Am. A., 5, (1988) 1058.

[24] T. Kondo, S. Matsuo, S. Juodkazis, and H. Misawa: Appl. Phys. Lett., 79, (2001) 725.

[25] J.H. Klein-Wiele and P. Simon: Appl. Phys. Lett., 83, (2003) 4707.

[26] K. Momoo, K. Sonda, Y. Nakata, and N. Miyanaga: Proc. Of SPIE., 8243, (2012) 82431E-1.

[27] A-M. Kietzig, M.N. Mirvakili, S. Kamal, P. Englezos, and S.G. Hatzikiriakos: J. Adhes. Sci. Technol., 25, (2011) 2789.

[28] H. Shimada, S. Kato, T. Watanabe, and M. Yamaguchi: Lasers Manuf. Process., 7, (2020) 496.

[29] M. Yamaguchi, S. Sasaki, S. Suzuki, and Y. Nakayama: J. Adhes. Sci. Technol., 29, (2014) 24.

[30] A.Y. Vorobyev and C. Guo: J. Appl. Phys., 117, (2015) 033103.

[31] M. Yamaguchi: Scientific Reports., 10, (2020) 2250.

(Received: June 4, 2021, Accepted: September 23, 2021)